Egyptian Knowledge Bank
https://ijmti.journals.ekb.eg/

International Journal of Materials Technology and Innovation
Volume 4, Issue 2 (2024), pages 14-29

Online ISSN 2682-4299

High-pressure hydrogen storage vessel designs for hydrogen embrittlement

Ashok Saxena[1,2]

[1]WireTough Cylinders, LLC, Bristol, VA

[2]University of Arkansas, Fayetteville, USA

*Corresponding author: E-mail: asaxena@wiretough.com

Received…….26 Oct.. 2024
Accepted……....5 Nov.2024
Published..……..31 Dec. 2024

Abstract

Storing gaseous hydrogen safely and economically at 35 to 70 MPa pressures is one of the few viable options for long-duration energy storage. The service duty cycles endured by the pressure vessels result in high fatigue stresses that determine their design life or inspection intervals. Hydrogen-assisted fatigue crack growth rate (HA-FCGR) due to hydrogen embrittlement exacerbates this and causes increases in the fatigue crack growth rates in pressure vessel steels by as much as 20 times. A phenomenological model that predicts the crack growth rate behavior as a function of ΔK, load ratio, R, and hydrogen pressure, P_{H_2}, is used to assess the designs of all steel, Type 1, and wire-wrapped, Type 2 vessels. Digital twins of Type 1 and Type 2 vessels are proposed for comparing the two design concepts over a broad pressure range using simulated service loading conditions in actual vessel sizes. Wire-wrapped Type 2 cylinders show significant advantages over Type 1 cylinders. At a storage pressure of 500 bar, the wire-wrapped pressure vessels save 33% in storage space, and 33% in materials' cost, and can store 155% more hydrogen compared to Type 1 vessels of similar exterior dimensions. These advantages increase further with a storage pressure of 700 bar, compared to lower pressures.

Keywords: ferritic steels, pressure vessels, design optimization, hydrogen storage, hydrogen-assisted cracking.

1. Introduction

Reducing hot gas emissions and CO_2 is a global challenge and requires collective action from all nations [1-3]. The alarm bells are already sounding, so the future that we are speaking of is not that far away! The phrase, "think globally and act locally" has more relevance than ever in dealing with environmental challenges. Technical solutions to problems exist, and more are being developed rapidly; however, implementation requires attitudinal changes and business incentives that only change gradually. It is thus important to pursue changes when the opportunity arises and to implement them when they are least disruptive. For example, as new power plants are planned to meet the increasing global energy demand, we must prioritize building renewable energy power plants.

Renewable power such as wind, solar, geothermal, etc. have different requirements and their suitability depends on geographical factors so no one solution fits all. All renewable energy plants produce variable amounts of energy during a single day, which is not always in phase with the demand. Similarly, fossil-fuel electricity-generating plants are shut down frequently and ramped up rapidly to manage variable energy demands within a single day. Damage to plant equipment/components due

IJMTI vol. 4, issue 2 (2024) 14-29 https:// doi: 10.21608/IJMTI.2024.331423.1113

to thermal cycling causes unplanned outages that can be expensive and result in inefficient energy conversion. Integrating an onsite environment-friendly energy storage facility addresses this challenge. The ideal scenario is to produce as much energy as possible during all periods including when the demand is low and store the excess energy for use during peak demand periods. Hydrogen has several advantages in becoming an important means of long-duration energy storage (LDES) [1,2]. It is clean when derived from green sources and has a high gravimetric energy density of 140 MJ per KG compared to gasoline's 46 MJ/KG [4]. However, larger amounts of space are needed to store hydrogen compared to the space needed to store the equivalent amount of energy as liquid fossil fuels [4]. Thus, hydrogen is only viable for LDES if it is highly compressed (35 -70 MPa) to reduce the space requirement. Advances in pressure vessel technology are needed to make hydrogen at high pressures economically viable and safe on a large scale.

Hydrogen is known to cause embrittlement in ferritic steels, which are the most cost-effective materials for pressure vessels [4-8]. Thus, the hydrogen-assisted fatigue crack growth rate (HA-FCGR) behavior of pressure vessel steels in high-pressure hydrogen is a front-end consideration in the design of pressure vessels for storing hydrogen and estimating their design/remaining life and safe inspection intervals.

In this study, the question addressed is how to design pressure vessels for storing hydrogen at high pressures that are safe and are assured to not fail during the intended service lifetime. Models based on recent phenomenological understanding of the kinetics of hydrogen embrittlement developed for characterizing and predicting the behavior of simulated cracks or crack-like defects that are exposed to high-pressure hydrogen are used in the analysis. Two types of pressure vessel designs are compared and quantitatively assessed using digital twins that respectively represent them. The first kind of design is a Type 1 vessel swaged from a seamless pipe, while the second design is a Type 2 cylinder classified as a composite vessel that utilizes a thinner wall Type 1 vessel as core and is hoop wrapped with high strength fibers or steel wires.

1. DESIGN CONSIDERATIONS AND OPTIMIZATION USING DIGITAL TWINS

The subsequent discussion considers design considerations in hydrogen storage vessels for ground-storage applications, such as in central hydrogen hubs and in refueling stations for cars, buses, and trucks. These include safety, cost, fatigue endurance, facility space requirements, and the frequency of nondestructive inspections of the vessels during service to extend their life beyond the initial design life. The vessel weight is a secondary consideration in this application; however, it is closely tied to several other primary considerations such as cost, material conservation, and energy conservation making it just as important as the other main considerations.

Digital twins are a tool for modeling the behavior of a physical system that enables one to simulate complex interactions of variables that affect their performance. It is a tool for gaining insights and making predictions that assist in decision making. This paper uses "digital twins" to comprehensively assess the designs of Type 1 and Type 2 pressure vessels for storing hydrogen at high pressures in ground storage applications. In both designs, ferritic pressure vessel steels are in contact with gaseous hydrogen at high pressures, so their performance under these conditions is most relevant. This aspect is fully embedded in the digital twin model of the two types of cylinders.

2.1 Digital Twin Models for Type 1 and Type 2 Storage Vessels

The digital twin model must realistically capture the most important design features and be amenable to virtual testing under simulated service conditions. Digital twins are proposed for Type 1 and Type 2 cylinders that enable quantitative comparisons between the two designs using a common set of service-related metrics and parameters.

Type 1 vessels consist of a cylinder made from a single seamless pipe with swaged ends to form the dome and the nozzles. The picture of a typical Type 1 vessel is shown in Fig.1a and the cross-section of the central region of the vessel is shown in Fig. 1b.

Type 2 vessels, Figs, 1c and 1d, consist of a Type 1 vessel used as a thin-wall liner that is circumferentially wrapped with several layers of glass or graphite fibers, or ultra-high-strength steel wires along the length of the vessel. The wrap reduces the hoop stresses in the liner walls. It also allows the vessels to be autofrettaged during manufacturing to retain high compressive stresses in the wall of the liner.

The cross-sections of the central region of the vessels, Figs 1b and 1d serve as the digital twins for Type 1 and Type 2 vessels, respectively. In both cases, the vessels are assumed to be infinitely long for analytical purposes; thus, the length, L >> OD (outside diameter of the vessel).

IJMTI vol. 4, issue 2 (2024) 14-29 https:// doi: 10.21608/IJMTI.2024.331423.1113

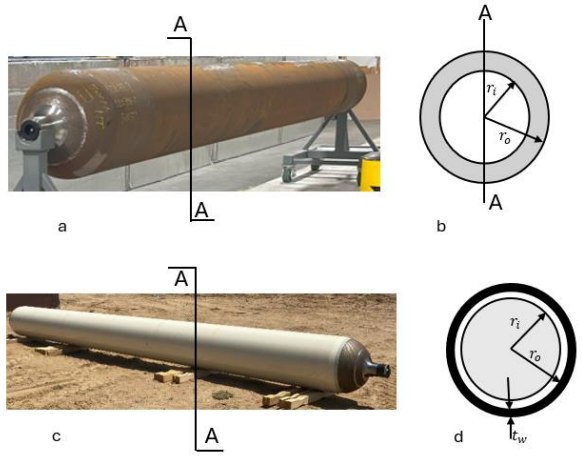

Fig. 1 (a) Picture of a Type 1 steel cylinder (b) a schematic of the cross-section in the central region of the cylinder (c) picture of a Type 2 cylinder in which a Type 1 cylinder is hoop wrapped with a jacket made of several layers of high strength steel wires (d) a schematic of the cross-section of the central region of the Type 2 cylinder.

The American Society of Mechanical Engineers (ASME) publishes codes of design practice for pressure vessels through its Boiler and Pressure Vessel Committee. This code specifies the design standards that must be met by all pressure vessels for ground storage of gases at high pressures. The design-by-analysis approach requires the consideration of postulated cracks at high-stress locations [6]. The assumed defects are of the size that could escape detection during nondestructive evaluation. A semi-elliptical, radial-axial surface crack on the interior wall of the vessel is used as such a flaw because it is life-limiting. The crack is assumed to be 1 mm deep and 5 mm long on the surface and is fully exposed to the hydrogen environment. Figure 2 shows the postulated flaws that are an integral part of the digital twin model, where,

r_i = internal radius of the cylinder/liner
r_o = outer radius of the cylinder/liner
$t = r_o - r_i$ = wall thickness of the cylinder/liner
t_w = thickness of the wrap in the case of Type 2 vessels
L = length of the cylinder

The length of the straight cylindrical section of the cylinder is held constant at 9 m and the cylinder length associated with the domes and the nozzles is in addition to the 9m. The overall length of the cylinders is less than 10 m to fit into standard tube trailers used for transporting gases. It can be increased or decreased without changing the substantial conclusions of this study. The fracture mechanics model for evaluating the fatigue life in the presence of hypothetical flaws is shown in Fig. 2. In the case of Type 1 cylinders, the external pressure, p_o, is 0 and for the Type 2 cylinders, it is the pressure exerted by the wrap on the liner's outer surface, and p_i is the internal pressure of the contained hydrogen. The loading for Type 2 cylinders also consists of the residual stresses in the liner due to the autofrettage process.

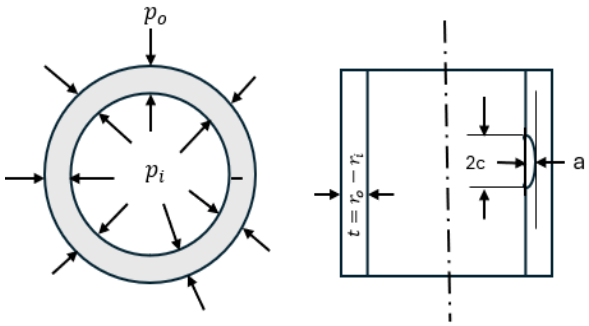

Fig. 2 Fracture mechanics model consisting of a hypothetical radial-axial flaw in the main body of the cylinder for Type 1 vessels and in the liner for Type 2 vessels

Construction Materials

Type 1 cylinders and metal liners used in Type 2 cylinders are typically made from SA 372 (or ASTM A372) Grade J or E, Class 70 steel [10,11]. The material chemistry is shown in Table 1, and the typical mechanical properties are shown in Table 2. The microstructure of these steels consists of tempered martensite resulting from an oil-quenched and tempered low alloy, medium carbon alloy steel. The minimum liner wall thickness in Type 2 liners must be such that the burst pressure exceeds 1.2 times the design pressure which should be at least 10% higher than the maximum operating pressure (MOP). The burst pressure, P_b, is estimated by Faupel's formula [12] given by the following equation.

$$P_b = \frac{2}{\sqrt{3}} S_y \left[2 - \frac{S_y}{S_u}\right] ln \frac{r_o}{r_i} \quad (1)$$

S_y = 0.2% yield strength, S_u = ultimate tensile strength

. The wrap consists of several layers of SA905 high-strength carbon steel wire. This is made from low-carbon steel and cold-drawn from a billet into a fine wire with a

IJMTI vol. 4, issue 2 (2024) 14-29 https:// doi: 10.21608/IJMTI.2024.331423.1113

diameter of 0.355 mm (0.014 in). The tensile strength of the wire exceeds 3.0 GPa and the percentage elongation is >12%. Tests on the wire material show that it does not degrade in the presence of low concentrations of hydrogen [10]. The wire layers that constitute the wrap are held together with epoxy, but the epoxy does not contribute to the strength of the jacket. The Type 2 design used in the analysis in this paper consists of wire wraps and has been referred to in the literature as the Type II-S design [11].

2.1 Stresses in Type 1 and Type 2 Internally Pressurized Cylinders

The well-known Lame's equations [13] for estimating the hoop stress in cylinders subjected to internal and external pressure were used. The circumferential stress, most relevant here, is given by equation (2) for the liner and equation (3) for the wire wrap that is treated as a thin wall cylinder:

$$\sigma_{\theta l} = \frac{p_i {r_i}^2 - p_o {r_o}^2}{{r_o}^2 - {r_i}^2} - \frac{{r_i}^2 {r_o}^2 (p_o - p_i)}{r^2 ({r_o}^2 - {r_i}^2)} \quad (2)$$

$$\sigma_{\theta w} = \frac{p_o r_o}{r_o - r_i} = \frac{p_o r_o}{t} \quad (3)$$

p_i = internal pressure of the contained hydrogen
p_o = contact pressure at the interface between the liner and the wrap
$\sigma_{\theta l}$ = hoop stress in the liner
$\sigma_{\theta w}$= hoop stress in the wire jacket

For Type 1 vessels, p_o= 0, in equation (1). For Type 2 vessels, the formula for estimating contact pressure, p_o, between the jacket and the liner was derived and is given in equation (4). This is the pressure that the wire jacket experiences on its ID and exerts on the OD of the liner. This is the mechanism by which the stress transfers from the liner to the wrap.

$$\frac{p_o}{p_i} = \alpha = \frac{[2{r_i}^2/({r_o}^2 - {r_i}^2)]}{\left[\frac{E r_o}{E_w t_w (1-\nu/2)} + \frac{{r_i}^2 + {r_o}^2}{{r_o}^2 - {r_i}^2}\right]} \quad (4)$$

The symbols used in equation (4) are as follows:

ν= Poisson's ratio for the liner material = 0.3
E = Young's modulus of the liner material
E_w = Young's modulus of the wire jacket
d = wire diameter
N = number of layers of wire used in the wrap, $t_w = Nd$

$\frac{p_o}{p_i} = \alpha$, is the pressure transfer ratio representing the fraction of the internal hydrogen pressure transferred from the steel liner to the steel wire wrap.

The value of α from equation (5) is shown in Fig. 3a,. As expected, it increases with the ratio of wrap thickness to the liner thickness, t_w/t but it also depends on the liner's thickness to inner radius ratio, t/r_i. It is higher for liners with higher radii for the same t_w/t as seen in Fig.3a. The pressure transfer ratio also depends strongly on the elastic modulus ratio, E_w / E of the wrap and the liner. In Fig. 3a, alpha values are plotted for $E_w / E = 0.7$ applied to Type 2 cylinders utilizing steel wires in the wrap [14]. Similar equations can also be derived for other elastic modulus ratios.

$$\alpha = \left(1 - 1.326\left(\frac{t}{r_i} - 0.0435\right)\right)\left(0.0066 + 0.4989\left(\frac{t_w}{t}\right) - 0.159\left(\frac{t_w}{t}\right)^2\right) \quad (5)$$

Figure 3b compares alpha values from equations (4) and (5) showing a strong alignment between the two equations.

2.2 Residual Stresses due to Autofrettage

In addition to the stress due to internal pressure, residual stress in the liners exists in Type 2 cylinders resulting from a step in the manufacturing process called autofrettage. The residual stresses due to autofrettage are given by equation (6) [14]. During autofrettage, the wrapped cylinder is subjected to an internal pressure that is sufficiently high to plastically deform the liner, while the wrap remains elastic. Upon removal of the pressure, the wrap exerts a high locked-in compressive circumferential stress on the liner wall.

The precise autofrettage pressure is chosen such that the equivalent strain on the OD of the liner is equal to the elastic strain for the stress level applied plus a plastic strain of 0.003 (or 0.3%) [14]. This ensures that the entire liner wall deforms plastically during autofrettage while the wrap remains elastic. The autofrettage pressure depends on the yield strength of the liner material (S_y), the thickness of the liner, t, the wrap thickness, t_w, and the inner radius of the liner. In equation (6), these parameters are referenced to their reference values designated by the subscript 0 [14] for a constant wrap thickness, $t_{wo} = 17.06\ mm$. Expressions can be derived for estimating the autofrettage pressure for other wrap thicknesses.

IJMTI vol. 4, issue 2 (2024) 14-29 https:// doi: 10.21608/IJMTI.2024.331423.1113

$$\frac{P_A}{P_{A0}} = \left(0.26 + 0.74\frac{S_y}{S_{y0}}\right)\left(.206 + .794\left(\frac{t}{t_0}\right)\right)\left(2.4 - 1.4\frac{r_o}{r_{00}}\right) \quad (6)$$

Where, $P_{A0} = 77\ MPa,\ S_{y0} = 482.5,\ r_{oo} = 308.5\ mm,\ t_0 = 22.9\ mm, t_{wo} = 17.06\ mm 22.9 \leq t \leq 25.2,\ 617 \leq D \leq 406,\ 482.5 \leq S_y \leq 703.5,$

Figure 4 shows the residual stress distribution following autofrettage for liners of different thicknesses and yield strengths for an OD of 617 mm($r_{00} = 308.5\ mm$) [14]. The compressive residual stresses are the highest in magnitude on the ID and lowest at the OD and are distributed linearly between the ID and OD. Since the autofrettage pressure is linked to a fixed amount of plastic deformation on the OD, the residual stress pattern for different thicknesses converges at that location. The magnitude of residual stress does not significantly depend on the liner thickness if the autofrettage pressure is chosen correctly. However, it depends significantly on the yield strength of the liner material.

Figure 5 shows the variation in residual stress distribution along the liner thickness for cylinders from liners with different ODs and yield strengths for a constant wrap thickness of 17.06 mm. The distribution of stress between ID and OD is assumed to be linear consistent with the observation from Fig. 4. The magnitude of residual stress changes significantly with the OD of the liner and the observation that the stress pattern is similar for liners with different thicknesses observed earlier for liners with an OD of 617 mm, also holds for the ODs of 508 mm and 406 mm.

Table 1 Chemical composition (weight %) of the metal liner (primary elements) and their standard ranges [10]

Element	C	Mn	P	S	Ni	Si	Cr	Mo	Cu	Al	Fe
ASME SA-372 Gr J Class 70 Standard	.35-.50	.75-1.05	<.025	<.025	-	.15-.35	.80-1.15	. 15-.25	-	-	Balance

Table 2 Tensile test results from an actual cylinder and comparison with standard values for SA372, Grade J, Class 70 steel. The specimens tested had a diameter of 12.33 mm (0.505 in) and a gage length of 50.8 mm (2 in) [10].

Material	0.2% Yield Strength, MPa (Ksi), S_y	Tensile Strength, MPa (Ksi), S_u	% Elongation	%Reduction in Area
Heat 315262	770.75 (111.8),	884.5 (128.3)	21.0	60.9
SA-372, Grade J Class 70 Standard	482.6 (70.0), min	827.3-930.7 (120-135)	18	-

IJMTI vol. 4, issue 2 (2024) 14-29 https:// doi: 10.21608/IJMTI.2024.331423.1113

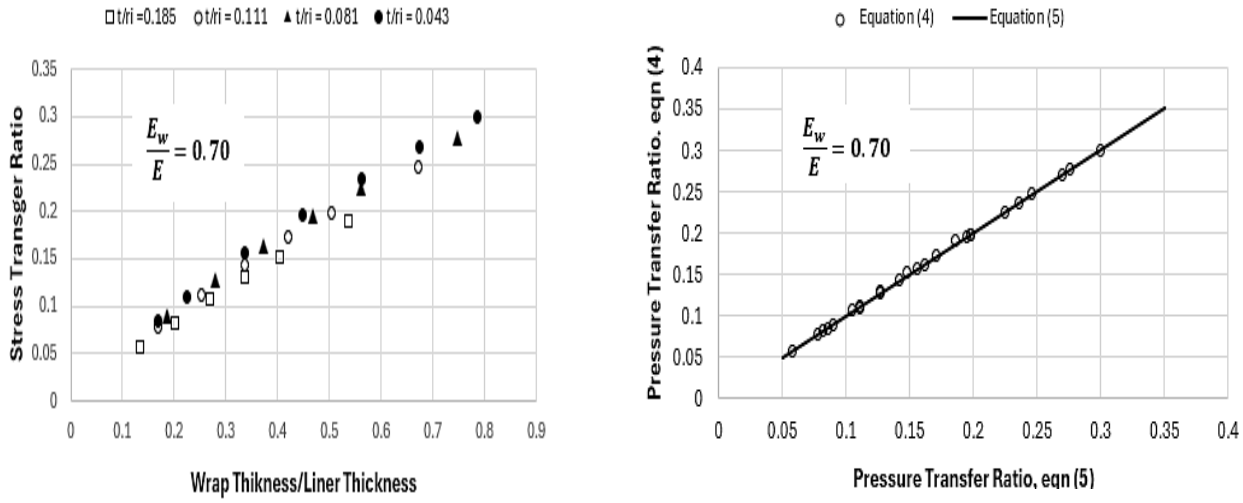

(a) (b)

Fig. 3 (a) Pressure transfer ratio as a function of t_w/t for liners of various sizes and (b) a comparison between the estimated values of the pressure transfer ratio from equation (4) with those from equation (5) for $E_{w//}E = 0.7$

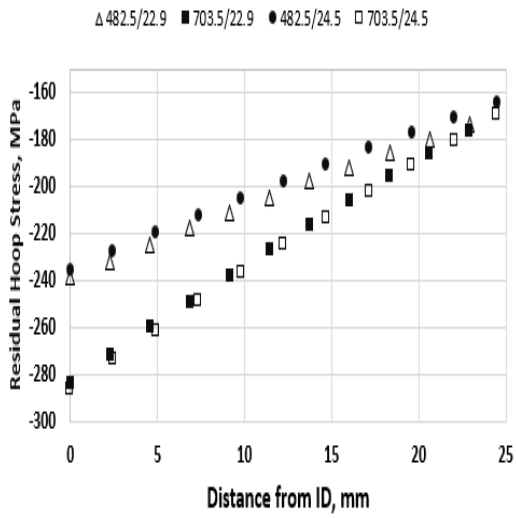

Fig. 4 The residual stress distribution in the liner wall following autofrettage. The analysis results are for liners with an OD of 617 mm and a wrap thickness of 17.06 mm [14].

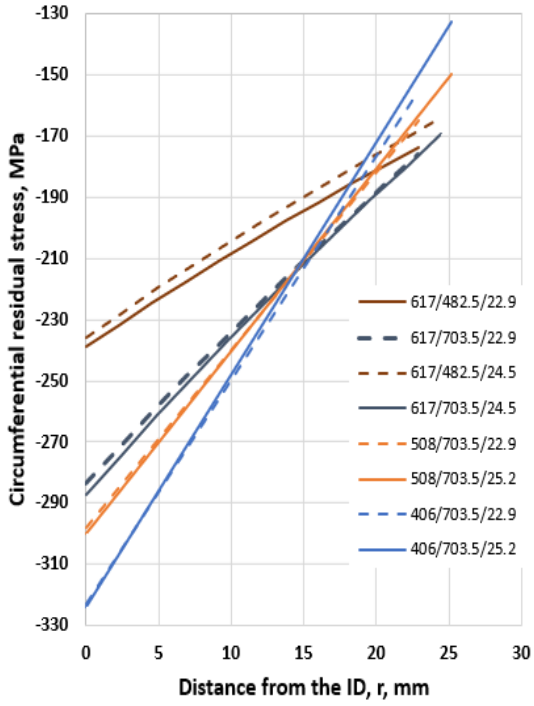

Fig. 5 The estimated circumferential residual stresses in liners of different outside diameters between 406 to 617 mm and wall thicknesses. The stresses do not vary significantly with wall thickness but vary with the yield strength of the liner material and the OD of the liner [14].

IJMTI vol. 4, issue 2 (2024) 14-29 https:// doi: 10.21608/IJMTI.2024.331423.1113

Equations (7) and (8) represent the residual compressive circumferential stress in the wall at the ID and OD of the liner, respectively. These equations account for the variation in residual stress due to yield strength, OD, and wrap thickness. As shown before, the ID residual stresses are not dependent on liner thickness, but the OD residual stresses vary with liner thickness.

$$\sigma_{\theta ID} = \sigma_{\theta IDo}\left(0.6 + 0.4\left(\frac{S_y}{S_{yo}}\right)\right)\left(1.4 - 0.4\frac{r_o}{r_{oo}}\right) \quad (7)$$

$$\sigma_{\theta OD} = \sigma_{\theta ID} - \left(-195 + 105\left(\frac{r_o}{r_{oo}}\right)\right)\frac{S_y}{S_{yo}}\frac{t}{t_0} \quad (8)$$

Where, $\sigma_{\theta ID}$ = circumferential stress at the ID of the liner, $\sigma_{\theta ID0}$= is the circumferential stress at the ID of the reference liner with a value of 238.84 MPa. Similarly, the reference values $S_{y0} = 482.5\ MPa$, $r_{00} = 308.5\ mm$. $t_0 = 22.9\ mm$.

Figures 6 and 7 show comparisons between the predicted residual circumferential stress at the ID and OD, respectively, for all cases analyzed by finite element analyses [14]. There is excellent agreement between the residual stresses predicted from equations (7) and (8) and those estimated by finite element analyses. In these figures, lines corresponding to an error band of ±5% are plotted to demonstrate that all predicted residual stresses lie within that error band.

2.3 Combined Autofrettage and Pressure Stresses in Type 2 Vessels

The combined circumferential stresses due to internal pressure during service and the residual stresses at the ID and OD due to autofrettage can be obtained by combining equations (2) and equations (7) and (8), respectively. These calculated values are compared in Fig. 8 with those obtained from finite element analyses [14] for identical conditions of OD = 617 mm, liner thickness of 22.9 mm, and wrap thickness of 17.06 mm. The equations seem to predict the stress at the ID almost perfectly and they somewhat overpredict the stress at the OD. The discrepancy is less than 5% in all cases which is acceptable for an approximate model, especially when it is conservative. These calculated stresses and their distributions are used in the design life calculations, described in Section 3.

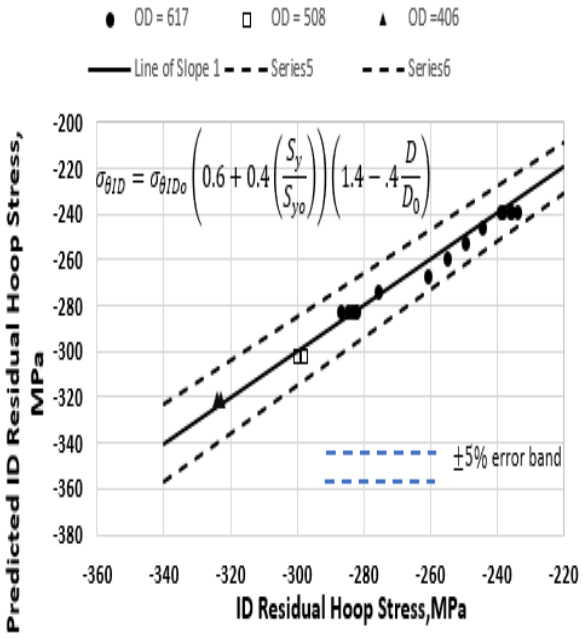

Fig. 6 Predicted residual circumferential stress at the ID from equation (7) and that calculated from the finite element analyses under similar conditions. Note that $D = 2r_o$ and $D_o = 2r_{oo}$ [14].

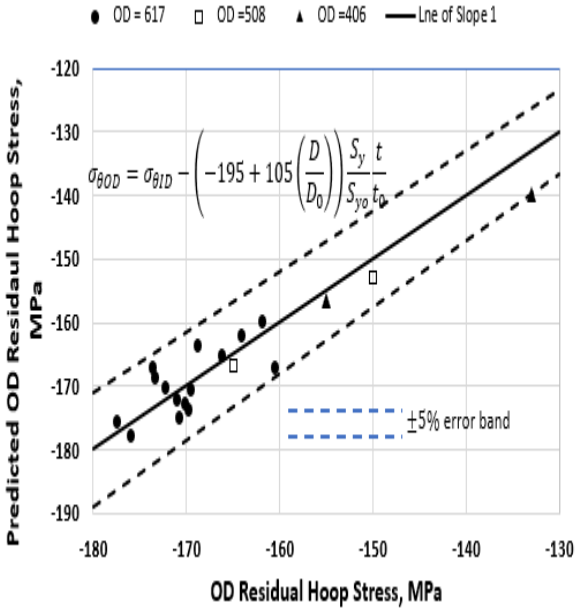

Fig. 7 Predicted residual circumferential stress at the OD from equation (8) and that estimated from the finite element analyses under similar conditions. Note that $D = 2r_o$ and $D_o = 2r_{oo}$ [14].

IJMTI vol. 4, issue 2 (2024) 14-29 https:// doi: 10.21608/IJMTI.2024.331423.1113

2.4 Hydrogen-Assisted Fatigue Crack Growth Behavior of Pressure Vessel Steels

The ASME master fatigue crack growth rate curve embedded in ASME Code Case 2938 was developed by San Marchi et al.[6]. This model was developed for a constant hydrogen pressure of 103 MPa and was derived from test data developed for load ratios, $R > 0$. A recent model developed by Saxena and Findley [15] has extended this equation to conditions of hydrogen pressures ranging from $0.02 \leq p \leq 103\ MPa$ and $-1 \leq R \leq 0.8$ that are more suitable for the design optimization of Type 2 cylinders subjected to autofrettage. The salient features of the modified model are as follows:

- Fatigue crack growth rates in A372 Grade J (or E) Class 70 steels with ultimate strength less than 950 MPa (137 Ksi) are relatively insensitive to the heat of steel and the yield strength. The data exhibit a knee in the da/dN versus ΔK trend at a ΔK equal to ΔK_c. The crack growth behavior at $\Delta K < \Delta K_c$ is classified as transient and the behavior at $\Delta K > \Delta K_c$ is called the steady-state region as shown in Fig. 9; ΔK_c depends on the load ratio, R. The slope in the Paris equation changes from a high value in the transient region to a smaller value in the steady-state region as also schematically shown in Fig. 9.

- The FCGR behavior in gaseous hydrogen increases significantly with load ratio, R, and the hydrogen pressure, P_{H_2}; thus, the effects of R and hydrogen pressure must be considered in calculating crack growth rates. Equations (9) and (10), represent the fatigue crack growth rate (FCGR) behavior of this class of steels for any load ratio, R $-1.0 \leq R \leq -0.8$ and hydrogen pressures of $0.02 \leq P_{H_2} \leq 103\ MPa$ [15]. In the transient regime the crack growth rate, $\left(\frac{da}{dN}\right)_{tr}$, is given by equation (9) and in the steady-state region, $\left(\frac{da}{dN}\right)_{ss}$, by equation (10). The crack growth rate at a given ΔK is the lower of the two values predicted by equations (9) and (10).

$$\left(\frac{da}{dN}\right)_{tr} = C_{10}\frac{1+0.43R}{1-R}(\Delta K)^{m_1} \quad (9)$$

$$\left(\frac{da}{dN}\right)_{ss} = C_{20}^{0}\left(1+\alpha_2\left(ln\frac{P_{H_2}}{0.02}\right)^{n_2}\right)\frac{1+2R}{1-R}(\Delta K)^{m_2} \quad (10)$$

We further define a load-ratio compensated HA-FCGR behavior, *da/dN**, by the following equations in the transient and steady-state regimes. *da/dN** is equivalent to the *da/dN* at $R = 0$.

$$\left(\frac{da^*}{dN}\right)_{tr} = \frac{\left(\frac{da}{dN}\right)_{tr}}{\left(\frac{1+0.43R}{1-R}\right)} = C_{10}(\Delta K)^{m_1} \quad (11)$$

$$\left(\frac{da^*}{dN}\right)_{ss} = \frac{\left(\frac{da}{dN}\right)_{ss}}{\frac{1+2R}{1-R}} = C_{20}^{0}\left(1+\alpha_2\left(ln\frac{P_{H_2}}{0.02}\right)^{n_2}\right)(\Delta K)^{m_2} \quad (12)$$

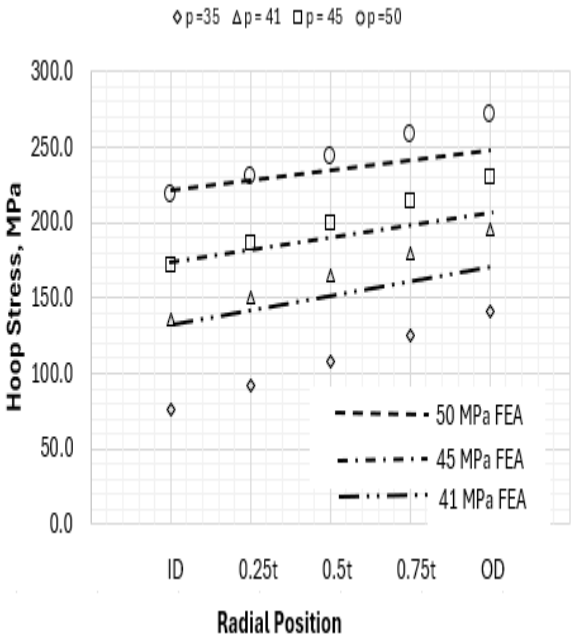

Fig. 8 Comparison between the circumferential stress predicted by the combination of equations (2), (7), and (8) and finite element analyses for various hydrogen pressures on cylinders with an OD of 617 mm.

The values of the various regression constants are listed in Table 3. The 95% confidence interval bands on the constants C_{10}, and C_{20}^{0} are also listed in the Table. Figure 10 shows the plots of HA-FCGR behavior predicted from equations (11) and (12) for the upper scatter band corresponding to the 95% confidence interval as a function of hydrogen pressure. Note from Fig. 10 that the crack growth rates in hydrogen are 4 to 20 times higher than in air, making hydrogen embrittlement the life-limiting material property in this application.

IJMTI vol. 4, issue 2 (2024) 14-29 https:// doi: 10.21608/IJMTI.2024.331423.1113

Table 3 Values of constants in equations (9) and (10). The da/dN is in mm/cycle and ΔK in $MPa\sqrt{m}$[15]

	C_{10}	m_1	CH_1		C_{20}^0	m_2	CH_2		n_2	α_2
			R ≥0	R≤ 0			R ≥0	R≤ 0		
mean	2.0 x10^{-11}	6.15	0.43	0	2.94x10^{-9}	3.219	2.0	0	4.2	0.0018
95% CI UB	3.94x10^{-11}	6.15	0.43	0	4.21x10^{-9}	3.219	2.0	0	4.2	0.0018
95% CI LB	1.01x10^{-11}	6.15	0.43	0	2.05x10^{-9}	3.219	2.0	0	4.2	0.0018

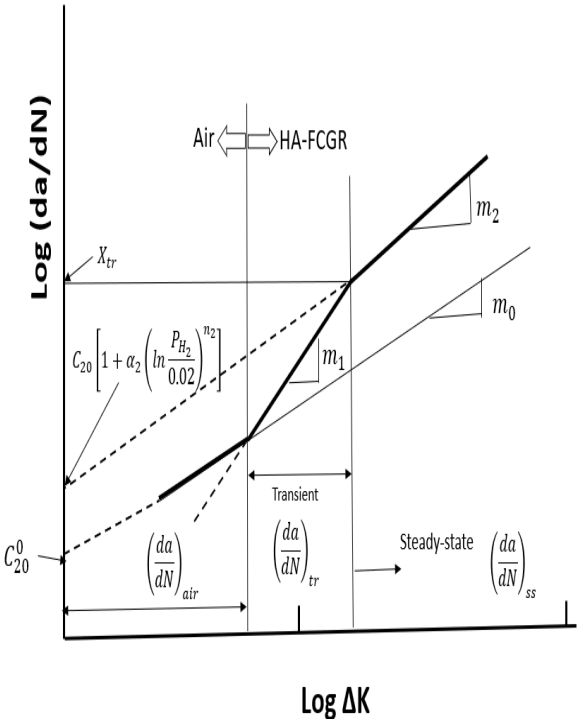

Fig. 9 Schematic representation of hydrogen-assisted fatigue crack growth behavior at constant pressure and load ratio observed in experimental HA-FCGR data along with the base line trend in air [15].

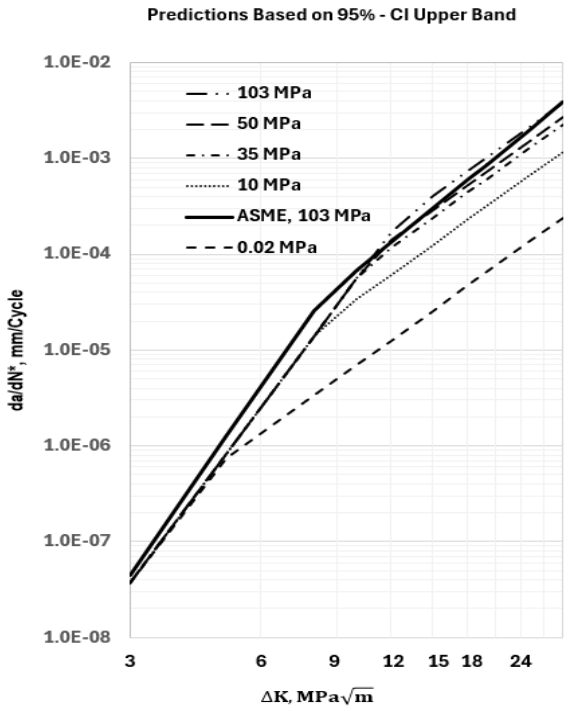

Fig. 10 Plots of 95% CI upper bound HA-FCGR predicted behavior from the model at various hydrogen pressures at an equivalent load ratio of 0. The solid black line is the trend from the ASME Section VIII- Division 3 model for a hydrogen pressure of 103 MPa at R = 0.

IJMTI vol. 4, issue 2 (2024) 14-29 https:// doi: 10.21608/IJMTI.2024.331423.1113

2.5 Stress Intensity Parameter Calculations

The K-expressions for Type 1 cylinders containing a hypothetical semi-elliptical surface flaw on the radial-axial plane located on the ID of the main body of the cylinder are given by the following equations from Newman and Raju [16].

$$K = \frac{p}{R_i t}\sqrt{\frac{\pi a}{Q}}F\left(\frac{a}{c},\frac{a}{t},\frac{t}{r_i},\phi\right)f_c \quad (13)$$

$$F = F_1 f_c g(\phi) f(\phi) \quad (14)$$

Where,

$$Q = 1 + 1.464(a/c)^{1.65} \text{ for a/c < 1} \quad (15a)$$

$$Q = 1 + 1.464(c/a)^{1.65} \text{ for a/c > 1} \quad (15b)$$

$$F_1 = 0.97[M_1 + M_2(a/t)^2 + M_3(a/t)^4] \quad (16)$$

$$M_1 = 1.13 - 0.09\frac{a}{c} \quad (17a)$$

$$M_2 = -0.54 + \frac{0.89}{0.2+\frac{a}{c}} \quad (17b)$$

$$M_3 = 0.5 - \frac{1}{0.65+\frac{a}{c}} + 14\left(1-\frac{a}{c}\right)^{24}$$

$$g(\phi) = 1 + \left[0.1 + 0.35\left(\frac{a}{t}\right)^2\right](1-sin\phi)^2 \quad (18)$$

$$f(\phi) = \left[sin^2\phi + \left(\frac{a}{c}\right)^2 cos^2\phi\right]^{1/4} \quad (19)$$

$$f_c = \left[\frac{r_o^2+r_i^2}{r_o^2-r_i^2} + 1 - 0.5\sqrt{\frac{a}{t}}\right]\frac{t}{r_i} \quad (20)$$

$$g(\phi = 0) = 1 + \left[0.1 + 0.35\left(\frac{a}{t}\right)^2\right]$$

$$g(\phi = \pi/2) = 1 \quad . \; f(\phi = 0) = \sqrt{\frac{a}{c}}$$

$$f(\phi = \pi/2) = 1$$

Next, the K-expressions for Type 2 cylinders are described. A semi-elliptical crack on the radial-axial plane on the ID of a long pipe is derived from a similar configuration, except in a flat plate [17]. The circumferential stress distribution along the radial direction in these cylinders as presented earlier in Fig. 4 is linear and is therefore well suited for being represented by a combination of uniform stress combined with bending. The K-expressions for a surface crack in a plate subject to tension and bending is given by equations (21) and (22).

$$K(\phi) = \left(\left(\sigma_t + P_{H_2}\right) + H\sigma_b\right)\sqrt{\frac{\pi a}{Q}}F_2\left(\frac{a}{c},\frac{a}{t},\frac{t}{r_i},\phi\right) \quad (21)$$

$$F_2 = [M_1 + M_2(a/t)^2 + M_3(a/t)^4]f(\phi) \quad (22)$$

Where,

$$\sigma_t = \frac{\sigma_{\theta OD} + \sigma_{\theta ID}}{2}; \quad \sigma_b = \frac{\sigma_{\theta ID} - \sigma_{\theta OD}}{2}$$

$$H = H_1 + (H_2 - H_1)sin^{\omega}\phi$$

$$\omega = 0.2 + \frac{a}{c} + 0.6\left(\frac{a}{t}\right)$$

$$H_1 = 1 - 0.34\left(\frac{a}{t}\right) - 0.11\left(\frac{a}{c}\right)\left(\frac{a}{t}\right)$$

$$H_2 = 1 + G_1\left(\frac{a}{t}\right) + G_2\left(\frac{a}{t}\right)^2$$

$$G_1 = -1.22 - 012\left(\frac{a}{c}\right)$$

$$G_2 = 0.55 - 1.05\left(\frac{a}{c}\right)^{3/4} + 0.47\left(\frac{a}{c}\right)^{3/2}$$

For ϕ= 0, $H = H_1$ and for ϕ= 90^0, $H = H_2$.

Also, for $R < 0$, $\Delta K = K_{max}$ and for R ≥ 0, $\Delta K = K_{max} - K_{min}$.

The accuracy of the *K*-expressions, equations (21) and (22) were verified against more accurate but more complicated expressions from reference [18]. The K-values from the two approaches are compared in Fig. 11 for some specific cases and found to be quite comparable, especially in the depth direction, *K*(90), which is more critical than the length direction of the flaw for determining lives.

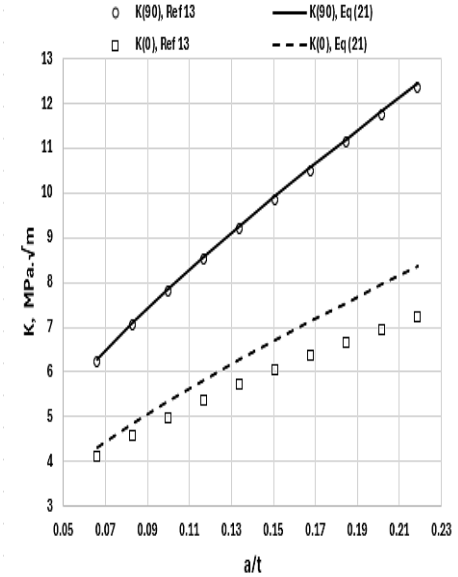

Fig. 11 Comparison of stress intensity parameters estimated from equation (21) and that from a more accurate expression from [14] for a Type 2 cylinder with a liner OD of 610 mm and ID of 580 mm pressurized to 350 bar. The a/c ratio assumed was 0.4.

IJMTI vol. 4, issue 2 (2024) 14-29 https:// doi: 10.21608/IJMTI.2024.331423.1113

2.6 Design Life/ Recommended Inspection Interval Estimation

Ground storage vessels are high-cost, capital-expense items; thus, durability and maintenance costs during their lifetimes are relevant considerations. Further, the vessels should be retired only for cause, and not because their original design life is exhausted. To ensure safety, inspection intervals must be determined using fracture mechanics methodology. The largest semi-elliptical flaw that can escape nondestructive inspection (NDI) is assumed to be 1 mm deep and 5 mm long on the ID surface as per current industry standards. We then estimate the number of cycles needed for a flaw of that size to grow to a critical size using the following equations

$$\frac{da_i}{dN} = f(\Delta K_{ai})$$

$$\Delta N_i(a_i) = \int_{a_i}^{a_i+\Delta a} \frac{da}{f(\Delta K_{ai})} \frac{dc_i}{dN} = f(\Delta K_{ci})$$

$$\Delta c_i = \frac{dc_i}{dN} \Delta N_i$$

$$c_{i+1} = c_i + \Delta c_i$$

$$N_f = \sum_{a_0}^{a_f} \Delta N_i(a_i) \quad (23)$$

Where, Δa = incremental change in the crack depth, a_0 = crack depth of a flaw that can escape detection and $2c_0$ is the corresponding crack length on the surface, ΔK_{ai} = the cyclic stress intensity parameter corresponding to the crack depth of a_i, ΔK_{ci} = the cyclic stress intensity parameter along the length of the flaw corresponding to half crack length c_i.

The design life/inspection interval, $N_{D,}$ is the smaller of the number of accumulated fatigue cycles corresponding to the crack size of $a = a_0 + 0.25(a_f - a_0)$, N_{D1}, and $N_f/2$, where N_f= the number of cycles needed for the crack to grow to a_f, the crack size corresponding to the value of K is equal to the threshold K-level for the onset of hydrogen-enhanced cracking under sustained loading.

Figure 12 shows an example plot of crack depth and half-crack length, c, as a function of accumulated cycles in a Type 1 cylinder, and how the design life, N_D is estimated. This procedure is recommended in the ASME design code and is widely accepted [6].

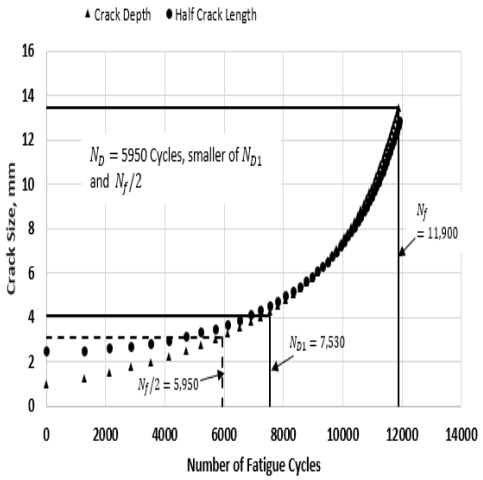

Fig. 12 A sample plot of crack depth and half-length with cycles for a Type 1 cylinder and how the design life is estimated.

3 RESULTS AND DISCUSSION

This section assesses the Type 1 and the steel wire-wrapped Type 2 pressure vessels using the digital twins discussed in the previous section. The vessels are designed to address the following needs of the hydrogen storage industry.

- The maximum operating pressures range from 200 to 700 bar with intermediate pressures of 250, 300, 350, and 500 bar. The nominal storage temperature is 25 ^{0}C (77^{0}F).
- The vessel length is 9000 mm in the straight section in all cases and has domes and nozzles on either side of the cylinder. This length allows cylinders to be transported in tube trailers (< 10,000 mm).
- The wall thickness of the steel vessels in the case of Type 1 vessels is limited to 45 mm (1.75") due to the hardenability of ferritic steels that are used in fabricating the pressure vessels. The outside diameter of the vessel was selected to meet the design goals as follows:
  - to store the most amount of hydrogen in a single vessel to reduce the footprint of the storage facility. This was achieved by choosing the largest OD possible while meeting or exceeding the design goals,
  - to minimize the cylinder weight per KG of hydrogen stored which results in lowering manufacturing costs,
  - to achieve a minimum initial design life/ the recommended inspection interval of 6,000 cycles

IJMTI vol. 4, issue 2 (2024) 14-29 https:// doi: 10.21608/IJMTI.2024.331423.1113

(30 years @ 200 cycles/year) of pressurization and depressurization in the case of Type 1 vessels and a minimum of 20,000 cycles (100 years @ 200 cycles/year) for Type 2 vessels. The higher design life for Type 2 vessels is necessary because the portion of the vessel underneath the wrap cannot be inspected during service.

- Accordingly, the following metrics are used for comparing candidate designs.
  - The most amount of hydrogen that can be stored in a single cylinder,
  - weight of the vessel per KG of hydrogen stored,
  - number of cylinders required to store 1000 KG of hydrogen, typical for refueling stations,
  - cost of construction materials per KG of hydrogen stored.

EXCEL programs were developed to (i) estimate the weight and capacity of the vessels (ii) analyze the stresses in the wall of the cylinder using equations (2) to (8) (iii) estimate the design life of the vessel from equation (23) using the calculated stresses, the material properties for the appropriate loading and pressure conditions from equations (11) and (12), and the K-expressions, equations (13) and (21).

In the case of Type 1 cylinders, the OD of the cylinder was initially fixed at 610 mm and the wall thickness was varied to achieve the design life/inspection interval goal of 6000 cycles. If the required wall thickness exceeded 45 mm for an OD of 610 mm, the OD was decreased to achieve the 6000-cycle design life while limiting the wall thickness to 45 mm. Once the OD was established, ID was calculated for the wall thickness of 45 mm. The other parameters such as water capacity, amount of hydrogen stored, the cylinder weight, materials cost, and the weight per KG of hydrogen stored were calculated. The results are presented below. The maximum OD permitted for Type 1 and the liner OD for Type 2[1] cylinders remain constant at 610 mm for hydrogen pressures up to 350 bar, but decrease for higher pressures, as seen in Fig. 13. For Type 1 cylinders, the maximum allowable diameter decreases more rapidly than for Type 2 cylinders. Type 2 cylinders have a higher water capacity at all pressures than Type 1 cylinders; the capacity increases by 5% at 200 bar to 175% at 700 bar. Figure 14 shows the weight of hydrogen that can be stored in one Type 1 versus Type 2 cylinders, clearly showing the significant increase in the storage capacity with the use of Type 2 cylinders at pressures of 500 bar or higher compared to the Type 1 cylinders.

Suppose a typical refueling station for trucks and automobiles is equipped to store 1000 KG of hydrogen onsite. The number of Type 1 and wire-wrapped Type 2 cylinders required at the storage facility as a function of storage pressure is shown in Fig. 16. Since the length of all cylinders is approximately 10 m, the floor area of the facility will be proportional to the number of cylinders needed to store 1000 KG of hydrogen. The figure reinforces the high potential of the wire-wrapped Type 2 cylinders in saving space for LDES facilities, especially in high-population areas where real estate is at a premium. Figure 17 presents a bar chart comparing the weights of the cylinders per KG of hydrogen stored for the Type 1 and the wire-wound Type 2 cylinders. Even though cylinder weight is not an important metric for the ground storage of hydrogen, it does influence other important metrics such as the cost of materials, cost of energy used during manufacturing, and materials conservation. Wire wound Type 2 cylinders are lighter than their Type 1 counterpart. At storage pressure < 350 bar, Type 2 cylinders are about 15% lighter than Type 1 cylinders. At storage pressures of 500 and 700 bar, Type 2 cylinders are 50% and 110%, respectively lighter than their Type 1 counterparts

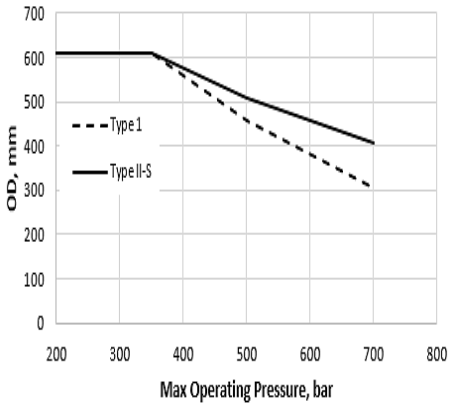

Fig. 13 Maximum OD for Type 1 and Type 2 cylinders as a function of hydrogen pressure for a design life/inspection interval of 30 years (or 6000 cycles) for Type 1 and 100 years for Type 2 (or II-S) cylinders, respectively. Higher ODs allow more hydrogen to be stored in a single vessel reducing the vessel weight per KG of hydrogen stored.

[1] Since the Type 2 cylinders in this study only had steel wraps, the term Type 2 is the same as Type II-S. Thus, the two terminologies are used interchangeably in this paper.

IJMTI vol. 4, issue 2 (2024) 14-29 https:// doi: 10.21608/IJMTI.2024.331423.1113

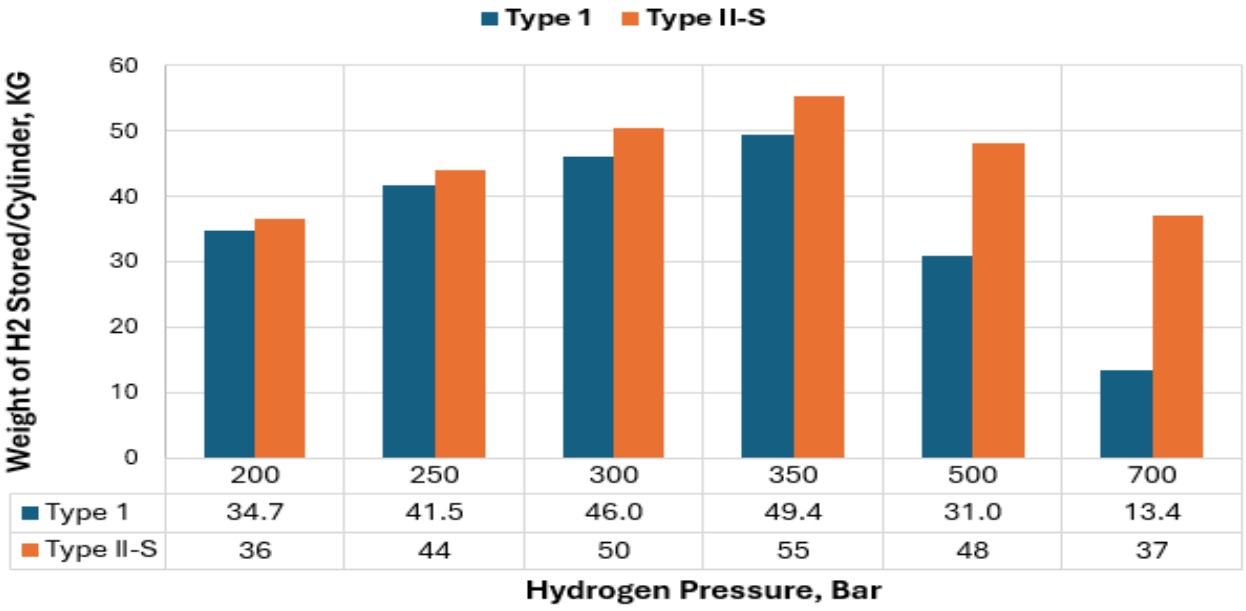

Fig. 14 The weight of hydrogen stored per cylinder in Type 1 and in wire wound Type 2 cylinders as a function of hydrogen pressure. Type 2 cylinders have a larger capacity for storing hydrogen compared to Type 1 cylinders.The cost advantages of wire-wound Type 2 cylinders significantly increase with storage pressure as shown in Fig. 15. The cost decreases are between 14% to 20% at pressures < 350 bar and are 55% and 120% at pressures of 500 and 700 bar, respectively.

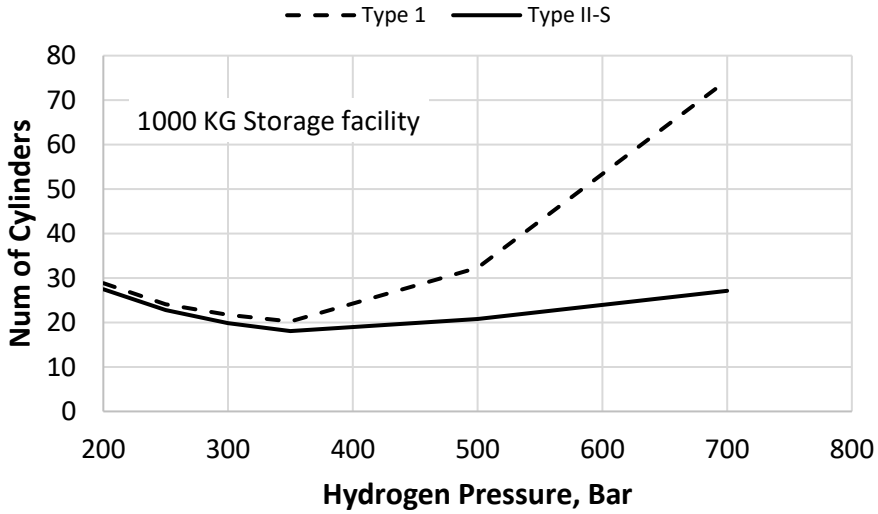

Fig. 15 Number of Type 1 and wire-wrapped Type 2 cylinders required for storing 1,000 KG of hydrogen as a function of storage pressure. The number of cylinders required to store a fixed amount of hydrogen relates to the space required to host the facility, so facilities utilizing Type 2 cylinders will have a smaller foot print compared to a facility based on Type 1 vessels.

IJMTI vol. 4, issue 2 (2024) 14-29 https:// doi: 10.21608/IJMTI.2024.331423.1113

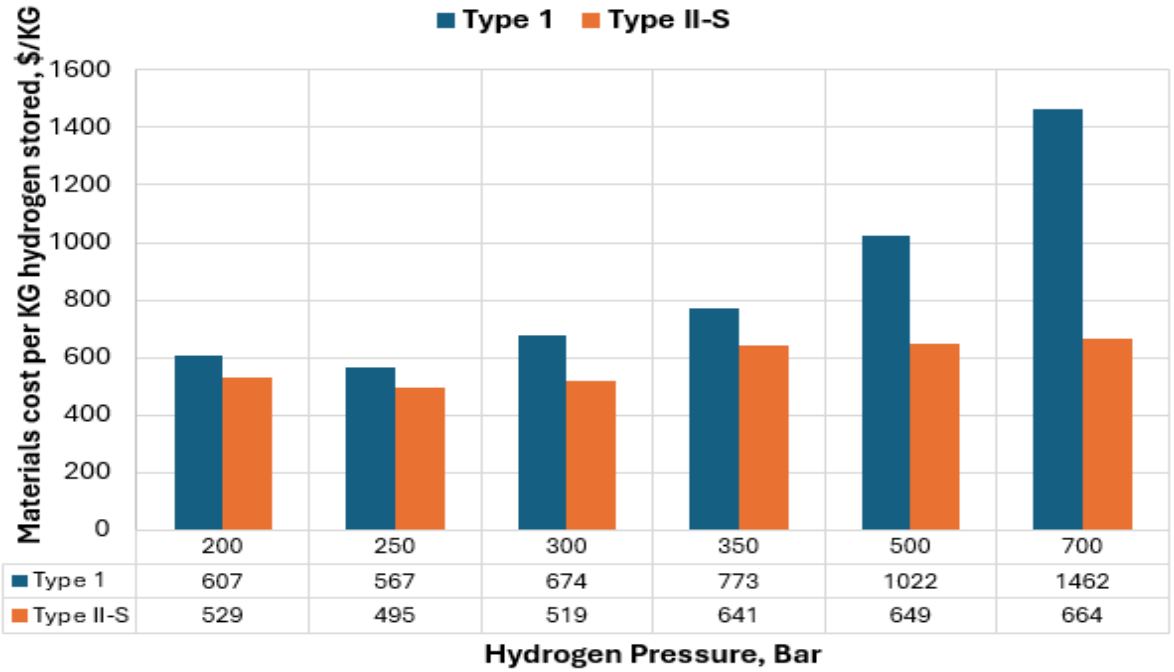

Fig. 16 Comparison of cost of materials per KG of hydrogen stored between Type 1 and Type 2 (or II-S) cylinders as a function of storage pressure. Type 2 (or II-S) cylinders save materials and processing costs compared to Type 1 cylinders.

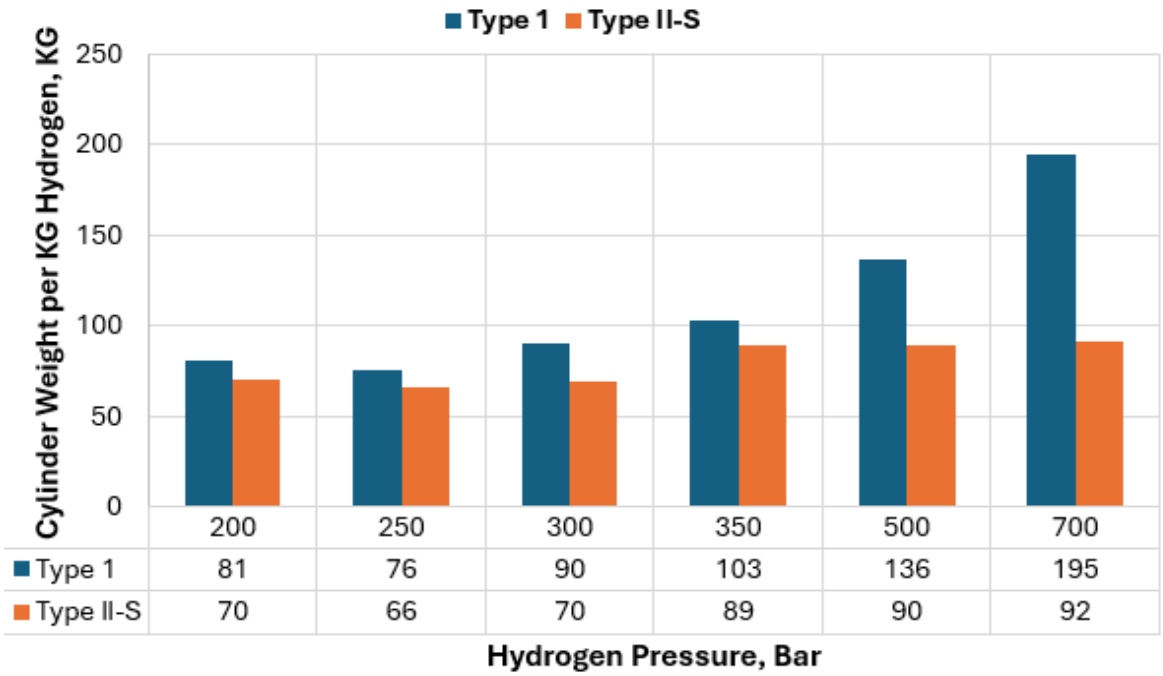

Fig. 17 Comparison of cylinder weight per KG of hydrogen stored between Type 1 and wire wound Type 2 cylinders. Type 2 cylinders are lighter compared to Type 1 cylinders.

IJMTI vol. 4, issue 2 (2024) 14-29 https:// doi: 10.21608/IJMTI.2024.331423.1113

4 CONCLUSIONS

The performance of Type 1 and wire-wound Type 2 cylinders for storing hydrogen in the operating pressure range of 200 to 700 bar is evaluated using their respective digital twins. The Type 2 cylinders were wrapped axially by several layers of ultra-high-strength wires and subsequently autofrettaged to enhance the fatigue crack growth life.

The following conclusions are drawn from the study:

- Use of wire wound Type 2 cylinders results in cost savings when compared with Type 1 cylinders. These savings increase with storage pressure. The cost savings are between 14% to 20% at pressures < 350 bar and rise to 55% and 120% at pressures of 500 and 700 bar, respectively
- The weight advantage of Type 2 cylinders in comparison to Type 1 cylinders expressed in KG per KG of hydrogen stored ranged between 15% at 200 bar to 110% at 700 bar.
- Storage facilities built to store 1000 KG of hydrogen based on Type 2 cylinders require 66% to 33% of the space needed for a facility utilizing Type 1 cylinders at pressures of 500 bar to 700 bar, respectively.
- Wire wound Type 2 cylinders are preferable to Type 1 at all pressures, but their advantages increase significantly for storage pressures greater than 350 bar.
- To keep up with the potential demand for Type 2 cylinders, it is necessary to bolster the manufacturing capabilities to produce them in large quantities.

ACKNOWLEDGEMENTS

The author gratefully acknowledges the partial support from the US Department of Energy through a grant, DE- EE0008828, where the Colorado School of Mines acted as the primary contractor. The partial support of WireTough Cylinders, LLC is also acknowledged as is the useful discussion with Prof. Kip Findley of the Colorado School of Mines.

REFERENCES

[1] Hydrogen Scaling up: A Sustainable Pathway for the Global Energy Transition." Hydrogen Council, https://hydrogencouncil.com/en/study-hydrogen-scaling-up/

[2] IEA (2022), Global Hydrogen Review 2022, IEA, Paris; https://www.iea.org/reports/global-hydrogen-review-2022, License: CC BY 4.0.

[3] Global Energy Perspective 2023: Hydrogen outlookhttps://www.mckinsey.com/industries/oil-and-gas/our-insights/global-energy-perspective-2023-hydrogen-outlook#/, McKinsey and Company, January 2024.

[4] Energy density – Wikipedia, https://en.wikipedia.org/wiki/Energy_density

[5] B.P. Somerday, P. Sofronis, K.A. Nibur, C. San Marchi, R. Kirchheim, "Elucidating the Variables Affecting Fatigue Crack Growth of Steels in Hydrogen Gas with Low Oxygen Concentrations", Acta Materialia, Vol. 61, 2013, pp 6153 – 6170.

[6] C. San Marchi, J. Ronevich, P. Bortot, Y., Wada, J. Felbaum, M. Rana, "Technical Basis for Master Curve for Fatigue Crack Growth of Ferritic Steels in High-Pressure Hydrogen in ASME Section VIII-3 Code", PVP 2019-93907, Proceedings of the ASME Pressure Vessels and Piping Conference, PVP 2019, July 14-19, 2019, San Antonio, Texas.

[7] J. Ronevich, C. San Marchi, K.A. Nibur, P., Bortot, G., Bassanini, and M. Sileo, "Measuring fatigue crack growth behavior of ferritic steels near threshold in high-pressure hydrogen gas", Proceedings of the ASME 2020 Pressure Vessels and Piping Conference, PVP2020-21263, July 19-24, 2020, Minneapolis, MN.

[8] C. San Marchi, and J.A. Ronevich, "Fatigue and Fracture of Pipeline Steels in High-Pressure Hydrogen", Proceedings of the ASME 2022 Pressure Vessel and Piping Conference, PVP 2022-84757, July 17-22, 2022, Las Vegas, NV.

[9] G. H. Koch, "Stress Corrosion Cracking and Hydrogen Embrittlement", in ASM Handbook, Lampman, S.E. Editor, Vol 19, Fatigue and Fracture, ASM International, Metals Park, OH, 1996, pp 483-506.

[10] A. Saxena, A. Prakash, G. R. Sharp, W. Thomson, T. David, F. Harless, I. Miller, V. Nagpal, J. Vain, D.T. Peters, C. Tipple, J. Milligan, K. Nibur, G. Romanoski, "Low-Cost Hydrogen Storage at 875 Bar Using Steel Liner and Steel Wire Wrap", Final Contract Report, DE-EE-0006668, WireTough Cylinders, December 2018.

[11] A. Saxena, F. Harless, C. Morrin, A. Beaver, S.B. Narasimhachary, L. Sripragash, T.L. Tang, D.T. Peters, K. Subramanian, and Erik

IJMTI vol. 4, issue 2 (2024) 14-29 https:// doi: 10.21608/IJMTI.2024.331423.1113

Ritter, "Durable Low-Cost Pressure Vessels for Bulk Hydrogen Storage", Final Contract Report, DE-FE-0032022, November 2023.

[12] T. Aseer Brabin, T. Christopher, B. N. Rao, "Bursting Pressure of Mild Steel Cylindrical Vessels", International Journal of Pressure Vessels and Piping, Volume 88, 2011, pp 119-122.

[13] S. Timoshenko, "Strength of Materials, Advanced Theory and Problems", D. Van Nostrand Co., New York, 1956,

[14] T. L. Tang, L. Sripragash, S.B. Narasimhachary, and A. Saxena, "A Model for Estimating the Autofrettage Pressure and Residual Stresses in Walls of Type 2 Pressure Vessels", Proceedings of the ASME 2023 Pressure Vessel and Piping Conference, PVP 2023- 105506, July 16 – 21, 2023, Atlanta, GA.

[15] A. Saxena and K.O. Findley, "A Model to Account for the Effects of Load Ratio and Hydrogen Pressure on the Fatigue Crack Growth Behavior of Pressure Vessel Steels", Vol.17, https://doi.org/10.3390/ma17174308.

[16] J.C. Newman and I.S. Raju, "Stress-Intensity Factors for Internal Surface Cracks in Cylindrical Pressure Vessels", Transactions of ASME, Vol 102, 1980, pp 342 – 346.

[17] J.C. Newman and I.S. Raju, "Analysis of Surface Cracks in Finite Plates Under Tension and Bending", NASA Technical Report 1578, 1979.

[18] J. Yamabe, H. Itoga, T. Awane, T. Matsuo, H. Matsunaga, "Pressure Cycle Testing of Cr-Mo Steel Pressure Vessels Subjected to Gaseous Hydrogen", Journal of Pressure Vessel Technology, Transactions of ASME, Vol. 136, 2016/011401, 13 pages.

.